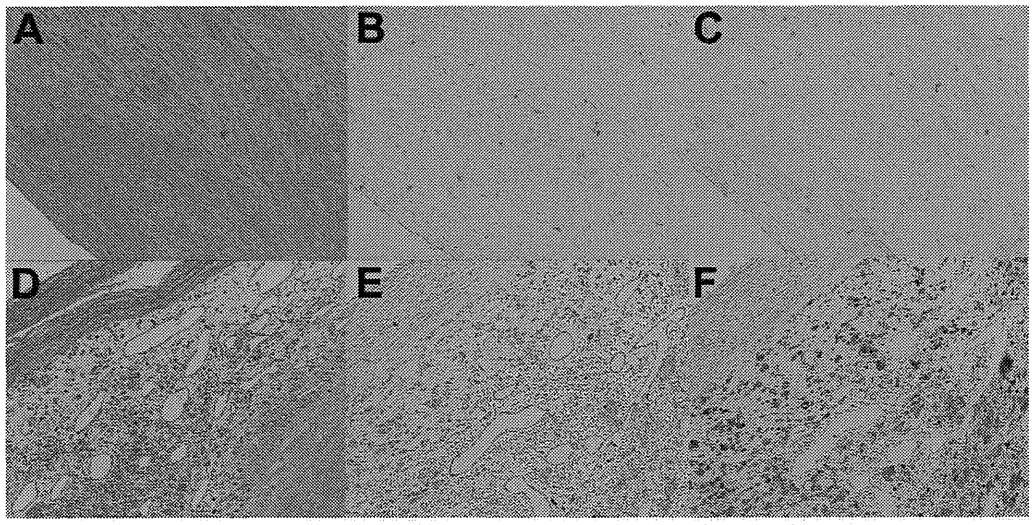

Figure 4. *Representative histochemical study for cases showing low (A-C, same case in Fig 1) and high BB-SIR (D-F, same case in Fig 2). Hematoxylin–eosin (A, D), CD31 (B, E), and CD68 (C, F) staining. Original magnification × 40.*

Microvessels stained by CD31 were significantly more frequently observed in the high–BB-SIR plaques (1.18 ± .90 vs. .51 ± .21/mm^2, respectively, $P = .026$; Fig 4, A-C, Fig 5, A), and CD68-positive cells were also significantly more prominent in the high–BB-SIR plaques (1010.9 ± 993.3 vs. 349.8 ± 240.5/mm^2, respectively, $P = .041$; Fig 4, D-F, Fig 5, B). The dorsal thickness of the carotid walls and plaques were rather thicker in the plaques of pattern B with first depiction of inner lumen compared with the plaques of pattern A (3.65 ± .78 vs. 1.90 ± .49 mm, respectively).

In the ICG videoangiography series, we consistently observed the delineation of the carotid lumen and wall first, followed by the depiction of vasa vasorum of the carotid wall (Figs 6 and 7). The time interval between the depiction of the carotid lumen/wall and the vasa vasorum was found to be slightly longer in the plaques with high–BB-SIR values than in those with low–BB-SIR values, with no significant difference (7.14 ± 1.68 vs. 6.20 ± 1.30 seconds, respectively; Fig 8). A significant difference was not found in the dorsal thickness of the plaques between the plaques with high– and low–BB-SIR values (2.75 ± 1.31 vs. 2.66 ± .88 mm, respectively).

Discussion

In the present study, we found that the FS videoangiography presented different patterns in terms of the depiction of adventitial vasa vasorum according to the cases, whereas the ICG videoangiography showed almost uniform patterns. The early depiction of adventitial vasa vasorum by the FS videoangiography was inversely associated with high–BB-SIR plaques, which were reported to have a tendency for intraplaque hemorrhage or symptoms.[8,9]

Three types of vasa vasorum were proposed in 1960 based on bovine aortic studies, that is, the vasa vasorum externae, internae, and venous vasa vasorum.[11] In the normal state, microvessels arising from the vasa vasorum are limited in adventitia and outer media and will not go beyond to intima.[12] Nevertheless, the development of the vasa vasorum and neovascularization in intima will be

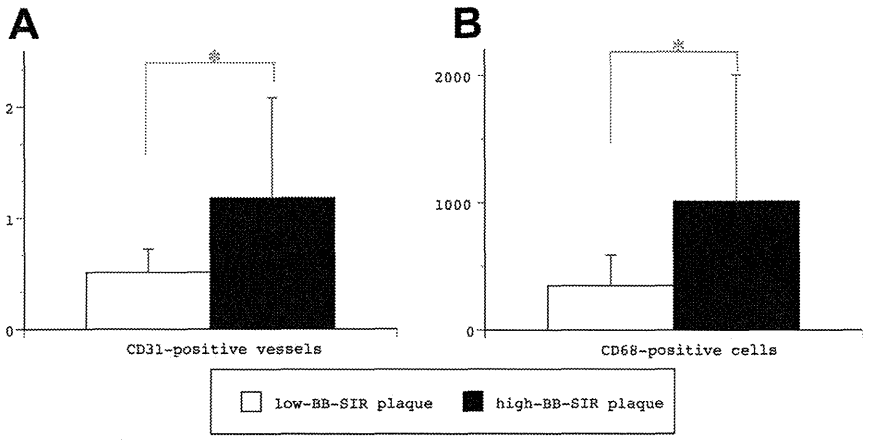

Figure 5. *(A) Microvessels stained by CD31 were more frequently observed in the high–BB-SIR plaques. (B) CD68-positive cells were also significantly more prominent in high–BB-SIR plaques, at* *P < .05.

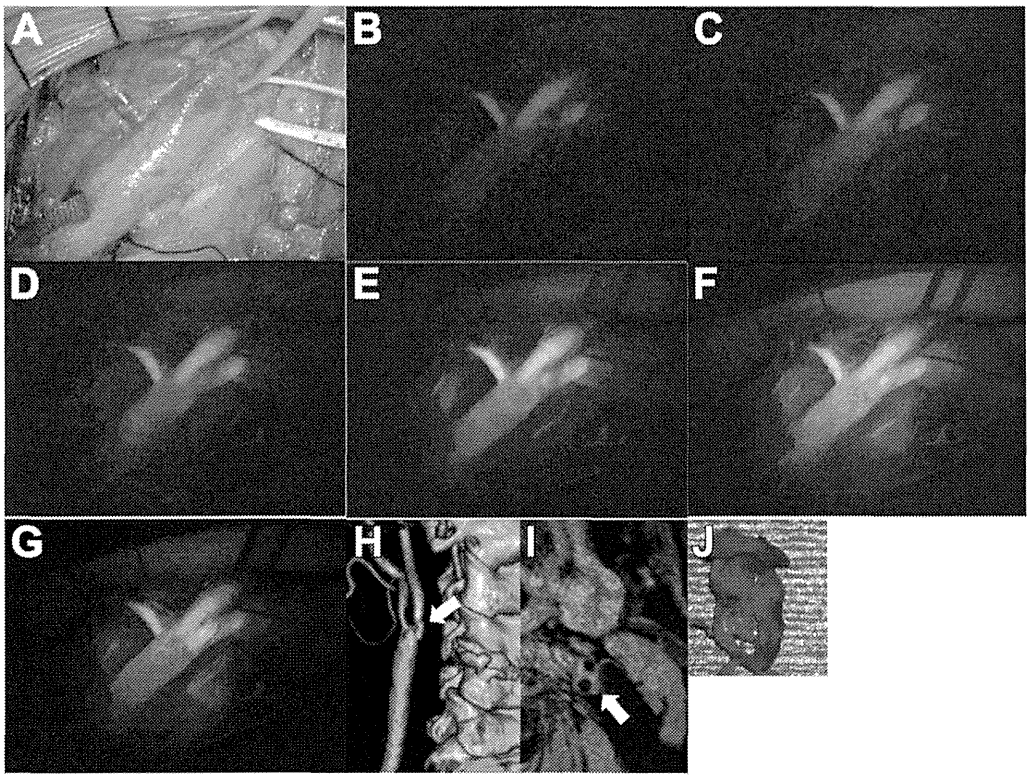

Figure 6. *A 69-year-old male with right asymptomatic carotid stenosis, as a representative case of low BB-SIR of carotid plaque (white arrow) for indocyanine green videoangiography. (A-G) Before and 1, 3, 5, 10, 20, and 30 seconds after the initial depiction, respectively. Delineation of the carotid lumen and wall was observed first, followed by the depiction of the vasa vasorum of the carotid wall (patter B). (H) Preoperative computed tomography angiography showing 72.0% stenosis (white arrow). (I) The BB-SIR was 1.07. (J) An extracted carotid fibrous plaque.*

recognized in progress with atherosclerosis. Several researchers reported that most of the microvessels were derived from adventitial vasa vasorum and seldom from intima or the luminal surface of the parent coronary artery.[13,14]

Fragile plaque neovessels with thin walls are prone to bleed, and intraplaque hemorrhage is considered an important event that evokes the rapid expansion and rupture of the plaque.[12] Abela[15] proposed that the formation and expansion of sharp-tipped cholesterol crystals within the necrotic core could readily cut through the vasa vasorum network, causing an intraplaque hemorrhage. The relationship between the dense network of the vasa vasorum along with a strong inflammatory reaction within the vascular wall and symptomatic atherosclerosis has been reported.[16]

Among the various MRI techniques used for plaque imaging,[17-19] the BB method is widely applied, and high–BB-SIR values have been shown to be associated with the density of microvessels in plaques as shown in the present study and thus with intraplaque hemorrhages and symptoms.[8,9,20]

We thus speculated that plaques with an early and dense depiction of adventitial vasa vasorum by FS videoangiography might be vulnerable and symptomatic because of microvessels derived from the vasa vasorum, showing high–BB-SIR values.

However, we found that the plaques with a delayed depiction of adventitial vasa vasorum by FS videoangiography in the present study actually showed higher BB-SIR values with denser microvessels and macrophages than the plaques with early vasa vasorum depiction, indicating that they were vulnerable and symptomatic. We then measured the dorsal thickness of plaques to test whether the thick wall interfered with the depiction of the inner lumen by duplex ultrasonography, which demonstrated that the thickness of the plaques did not affect the results in our study.

If neovascularization in carotid plaques, which elicits intraplaque hemorrhage is derived mainly from adventitial vasa vasorum as shown in previous studies concerning coronary arteries,[13,14] the adventitial vasa vasorum should have been depicted first and the arterial wall and lumen second in the culprit plaques. The results of the present study thus indicate that intimal neovascularization might be nourished by a supply route other than adventitial derivation. The possibilities naturally go to a supply that originates from the inner side by diversion or branching vessels (vasa vasorum interna[11,21]).

As for imaging of the vasa vasorum, not a few researchers reported the visualization of vasa vasorum using contrast-enhanced ultrasound and also demonstrated an association between the depiction of the vasa

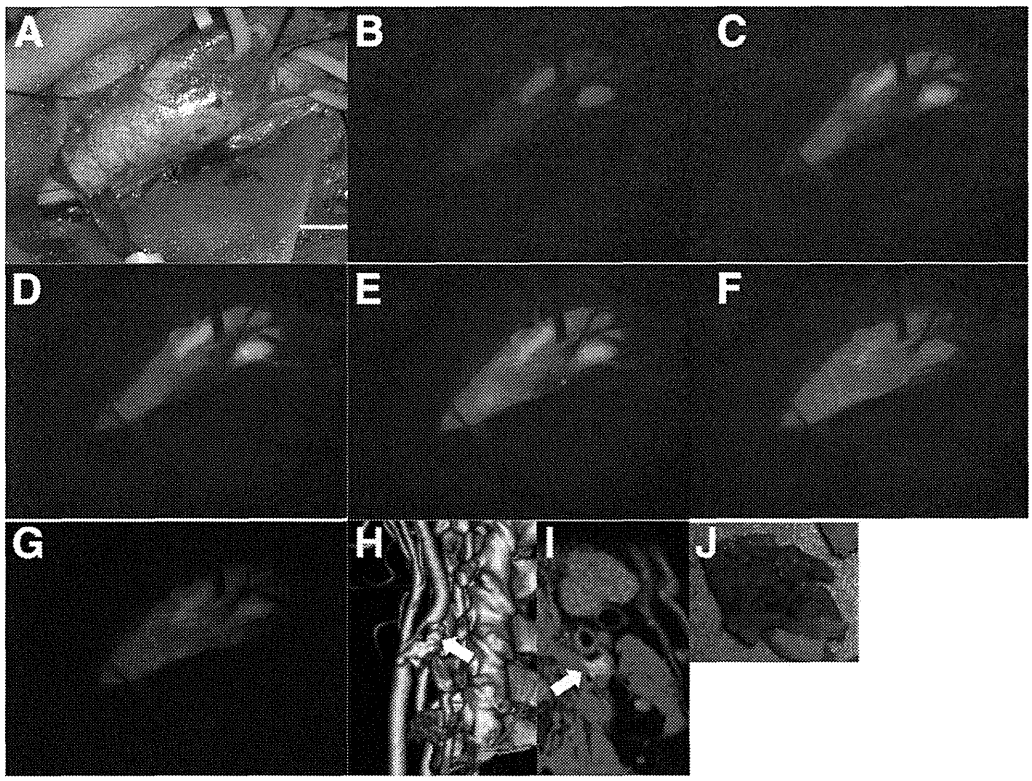

Figure 7. *A 70-year-old male with right asymptomatic carotid stenosis, as a representative case with high BB-SIR of carotid plaque (white arrow) for indocyanine green videoangiography indocyanine green videoangiography. (A-G) Before and 1, 3, 5, 10, 20, and 30 seconds after the initial depiction, respectively. Delineation of the carotid lumen and wall was constantly observed first, followed by the depiction of the vasa vasorum of the carotid wall (pattern B) as in the low–BB-SIR cases. (H) Preoperative computed tomography angiography showing 80.0% stenosis (white arrow). (I) The BB-SIR was 1.60. (J) An extracted carotid atheromatous plaque.*

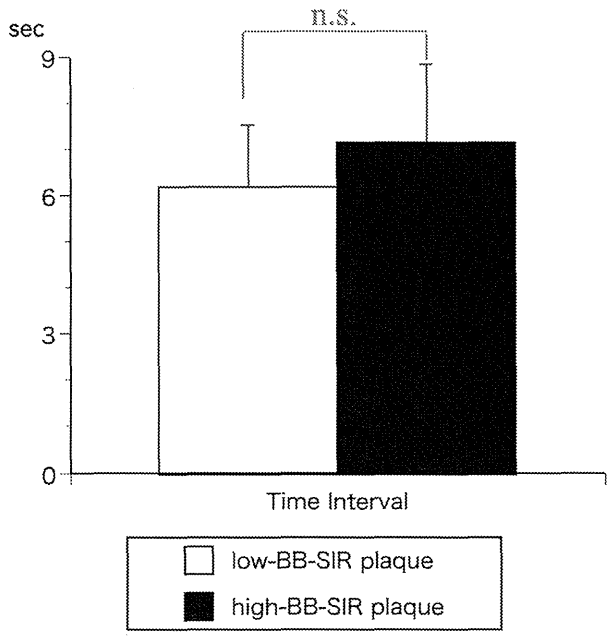

Figure 8. *The time interval between the depiction of the carotid lumen/wall and vasa vasorum was slightly but not significantly longer in the plaques with high BB-SIR than in those with low BB-SIR in indocyanine green videoangiography.*

vasorum and symptoms.[22-24] MRI was also used for depicting the vasa vasorum.[25,26] A few investigators described the state of the vasa vasorum using ICG videoangiography during CEA,[2] but seldom has this been reported with FS. Because ICG was "fluoro-lucent" to arterial wall because of its strong fluorescence signal (as shown in a previous study[27] and the present study), the lumen was inevitably visualized first. The vasa vasorum was observed later and relative good contrast was obtained in a few cases by the weak lumen augmentation at the site of severe stenosis with thick arteriosclerotic plaque.

In contrast, FS is fluoro-opaque to arterial walls compared with ICG, and this gives FS an advantage for observing the vasa vasorum on the carotid wall, although the confirmation of the site of the stenosis during CEA was inferior to that with ICG.[1,3] Although one of the researchers using ICG during CEA reported the presence of some plaques showing the preceding depiction of vasa vasorum,[2] it might already be at a later phase than the lumen/wall depiction, compared with the results obtained by FS videoangiography. Additionally, no significant difference was demonstrated in the interval of time required for emerging vasa vasorum between

plaques with low– and high–BB-SIR values in ICG videoangiography. The results of the present study thus demonstrate the distinctive potential of FS videoangiography for intraoperative plaque imaging focusing on the vasa vasorum and thus vulnerability of the plaque.

The main limitation of our study is the small sample size. Further studies with larger numbers of patients are warranted to clarify the issues examined here.

Conclusions

We found that not early but delayed detection of adventitial vasa vasorum in FS videoangiography corresponded with high–BB-SIR values and the density of neomicrovessels in plaques. The results indicated that intimal neovascularization in vulnerable plaques might be derived from the luminal side. The potential of intraoperative plaque imaging with FS videoangiography for detecting culprit plaques was also suggested.

Acknowledgment: We are grateful to Dr. Takayuki Ohno, Dr. Yusuke Nishikawa and all our ward staff for their invaluable clinical contributions.

References

1. Haga S, Nagata S, Uka A, et al. Near-infrared indocyanine green videoangiography for assessment of carotid endarterectomy. Acta Neurochir (Wien) 2011;153:1641-1644.
2. Kamiyama K, Nakagawara J, Takada H, et al. Transformation of the vasa vasorum from normal vessel structures to atheroma nutrient vessels on ICG angiography of cervical carotid artery stenosis. Surg Cereb Stroke (Jpn) 2011;39:413-419.
3. Lee CH, Jung YS, Yang HJ, et al. An innovative method for detecting surgical errors using indocyanine green angiography during carotid endarterectomy: a preliminary investigation. Acta Neurochir (Wien) 2012;154:67-73.
4. North American Symptomatic Carotid Endarterectomy Trial Collaborators. Beneficial effect of carotid endarterectomy in symptomatic patients with high-grade carotid stenosis. N Engl J Med 1991;325:445-453.
5. Executive Committee for the Asymptomatic Carotid Atherosclerosis Study. Endarterectomy for asymptomatic carotid artery stenosis. JAMA 1995;273:1421-1428.
6. Katano H, Yamada K. Comparison of internal shunts during carotid endarterectomy under routine shunting policy. Neurol Med Chir (Tokyo) 2013; http://dx.doi.org/10.2176/nmc.oa2013–0218. Epub ahead of print.
7. Miura T, Matsukawa N, Sakurai K, et al. Plaque vulnerability in internal carotid arteries with positive remodeling. Cerebrovasc Dis Extra 2011;1:54-65.
8. Yamada K, Yoshimura S, Kawasaki M, et al. Embolic complications after carotid artery stenting or carotid endarterectomy are associated with tissue characteristics of carotid plaques evaluated by magnetic resonance imaging. Atherosclerosis 2011;215:399-404.
9. Yoshida K, Narumi O, Chin M, et al. Characterization of carotid atherosclerosis and detection of soft plaque with use of black-blood MR imaging. AJNR 2008;29:868-874.
10. Katano H, Yamada K. Upregulation of ANGPTL4 messenger RNA and protein in severely calcified carotid plaque. J Stroke Cerebrovasc Dis 2014;23:933-947.
11. Schoenenberger F, Mueller A. On the vascularization of the bovine aortic wall. Helv Physiol Pharmacol Acta 1960;18:136-150.
12. Doyle B, Caplice N. Plaque neovascularization and antiangiogenic therapy for atherosclerosis. J Am Coll Cardiol 2007;49:2073-2080.
13. Kumamoto M, Nakashima Y, Sueishi K. Intimal neovascularization in human coronary atherosclerosis: its origin and pathophysiological significance. Hum Pathol 1995; 26:450-456.
14. Zhang Y, Cliff WJ, Schoefl GI, et al. Immunohistochemical study of intimal microvessels in coronary atherosclerosis. Am J Pathol 1993;143:164-172.
15. Abela GS. Cholesterol crystals piercing the arterial plaque and intima trigger local and systemic inflammation. J Clin Lipidol 2010;4:156-164.
16. Fleiner M, Kummer M, Mirlacher M, et al. Arterial neovascularization and inflammation in vulnerable patients: early and late signs of symptomatic atherosclerosis. Circulation 2004;110:2843-2850.
17. Honda M, Kitagawa N, Tsutsumi K, et al. High-resolution magnetic resonance imaging for detection of carotid plaques. Neurosurgery 2006;58:338-346.
18. Mono ML, Karameshev A, Slotboom J, et al. Plaque characteristics of asymptomatic carotid stenosis and risk of stroke. Cerebrovasc Dis 2012;34:343-350.
19. Yoshimura S, Yamada K, Kawasaki M, et al. High-intensity signal on time-of-flight magnetic resonance angiography indicates carotid plaques at high risk for cerebral embolism during stenting. Stroke 2011;42:3132-3137.
20. Balu N, Chu B, Hatsukami TS, et al. Comparison between 2D and 3D high-resolution black-blood techniques for carotid artery wall imaging in clinically significant atherosclerosis. J Magn Reson Imaging 2008;27:918-924.
21. Gössl M, Rosol M, Malyar NM, et al. Functional anatomy and hemodynamic characteristics of vasa vasorum in the walls of porcine coronary arteries. Anat Rec A Discov Mol Cell Evol Biol 2003;272:526-537.
22. Vicenzini E, Giannoni MF, Puccinelli F, et al. Detection of carotid adventitial vasa vasorum and plaque vascularization with ultrasound cadence contrast pulse sequencing technique and echo-contrast agent. Stroke 2007;38:2841-2843.
23. Huang PT, Huang FG, Zou CP, et al. Contrast-enhanced sonographic characteristics of neovascularization in carotid atherosclerotic plaques. J Clin Ultrasound 2008; 36:346-351.
24. Coli S, Magnoni M, Sangiorgi G, et al. Contrast-enhanced ultrasound imaging of intraplaque neovascularization in carotid arteries: correlation with histology and plaque echogenicity. J Am Coll Cardiol 2008;52:223-230.
25. Kawahara I, Morikawa M, Honda M, et al. High-resolution magnetic resonance imaging using gadolinium-based contrast agent for atherosclerotic carotid plaque. Surg Neurol 2007;68:60-65.
26. Kawahara I, Nakamoto M, Kitagawa N, et al. Potential of magnetic resonance plaque imaging using superparamagnetic particles of iron oxide for the detection of carotid plaque. Neurol Med Chir (Tokyo) 2008;48:157-161.
27. Suzuki K, Watanabe Y, Ichikawa T. Usefulness of intraoperative fluorescence cerebral angiography using fluorescein sodium. Surg Cereb Stroke (Jpn) 2009;37:240-245.

Surgical Treatment for Carotid Stenoses with Highly Calcified Plaques

Hiroyuki Katano, MD, PhD,*† Mitsuhito Mase, MD, PhD,* Yusuke Nishikawa, MD, PhD,* and Kazuo Yamada, MD, PhD*

Background: The aim of this study was to clarify both the present status of treatment for carotid stenosis with highly calcified plaques and the appropriate treatment. *Methods:* A total of 140 consecutive treatments for carotid stenoses (carotid endarterectomy [CEA]:carotid artery stenting [CAS] 81:59) were enrolled in the study. We classified the patients into low-calcified plaque (LCP) and high-calcified plaque (HCP) groups by calcium score, determined by a receiver operating characteristic analysis, and we compared the results after both treatments. *Results:* The mean degree of residual stenosis and improvement rates of the stenosis after CAS for the HCP group were 9.7% ± 13.3% and 87.0% ± 16.8%, respectively, whereas those for the LCP group were 1.7% ± 6.1% and 97.9% ± 7.9% (both $P < .001$). A multiple logistic regression analysis revealed that only the calcium score was an independent pre-CAS predictor of residual stenosis. Restenosis at 6 months was observed frequently in the HCP group after both CAS and CEA (18.8% and 20.0%, respectively). Cerebral hyperperfusion syndrome was observed in 2 cases of CAS, 1 for each plaque group. The 30-day and 6-month rates for any stroke or death after CAS were 2.3% and 12.5% for the LCP and HCP groups, respectively, whereas those after CEA were 1.6% and 0%. *Conclusions:* Carotid stenoses with HCP (calcium score ≥420) treated by CAS showed a disadvantage in the degree of stent expansion compared to carotid stenoses with LCP, suggesting that CEA may be recommended as a surgical option. **Key Words:** Calcification—carotid artery stenting—carotid endarterectomy—carotid stenosis.

After the approval of self-expanding stents with filter protection devices by the Japanese Ministry of Health Labor and Welfare in 2008,[1,2] the rate of postoperative ischemic complications with so-called "soft" vulnerable lipid-rich plaques temporarily increased in patients with carotid artery stenting (CAS) treated in Japan. The rate decreased after the application of appropriate embolic protection devices.[3,4] Therefore, one of the remaining problems concerning the treatment of carotid stenosis may concern instead the so-called "hard plaques" with calcification.

In a previous study, our pathologic and radiologic assessments suggested that severely calcified plaque might prevent the expansion of carotid stents and therefore affect the results of CAS,[5,6] and we recommended that physicians conduct a preoperative analysis of carotid plaque using the Agatston calcium score with multidetector computed tomography angiography (MDCTA).[7]

Nonaka et al[8] warned that calcification at carotid bifurcations is an independent risk factor for prolonged hypotension after CAS that might relate to periprocedural ischemic events. They described how plaque calcification

From the *Departments of Neurosurgery; and †Medical Informatics and Integrative Medicine, Nagoya City University Graduate School of Medical Sciences, Nagoya, Japan.

Received October 23, 2012; revision received November 24, 2012; accepted November 28, 2012.

Address correspondence to Hiroyuki Katano, MD, PhD, Department of Neurosurgery, Nagoya City University Graduate School of Medical Sciences, 1 Kawasumi, Mizuho-cho, Mizuho-ku, Nagoya 467-8601, Japan. E-mail: katano@med.nagoya-cu.ac.jp.

1052-3057/$ - see front matter

http://dx.doi.org/10.1016/j.jstrokecerebrovasdis.2012.11.019

might indicate increased baroreflex sensitivity[9] through the distortion and stretching of the carotid sinus. Chang et al[10] reported that the presence of calcified plaque on plain film was significantly associated with an increased rate of stent fracture or deformation, whereas Coppi et al[11] disclosed that calcification type III increased the odds of stent fracture 4.5-fold. Therefore, if carotid stenoses with high-calcified plaque (HCP) are treated with CAS, residual stenosis should be considered, not only because it might restrict expansion related to mechanical limitations of the self-expanding stent, but also to avoid additional excessive expansion that could elicit the unfavorable effect of postdilation to overcome the hardness of the calcified plaque.

In the present study, we set the threshold of the calcium score for HCP by creating a receiver operating characteristic (ROC) curve with respect to the degree of residual stenosis after CAS, and we compared the results of treatment of carotid stenosis by carotid endarterectomy (CEA) and CAS, for a patient group with low-calcified plaque (LCP) and an HCP group. We discuss the present status of treatment for carotid stenosis with HCP and what treatment is appropriate.

Methods

Patient Population and Surgical Treatments

A total of 140 consecutive treatments for carotid stenosis (ratio of CEA:CAS 81:59; mean degrees of stenosis 78.6% ± 12.2%) in 131 patients (mean age 70.7 ± 6.7 years) performed between June 2002 and December 2011 were examined. Patient data are summarized in Table 1.

Five patients had bilateral carotid stenoses; 3 were treated by CAS for both sides and the other 2 were treated on 1 side by CEA and the other by CAS. Four patients who underwent CEA developed restenosis and were retreated by CAS. Surgical indications for the treatment of carotid stenosis adhered to the criteria of the North American Symptomatic Carotid Endarterectomy Trial (NASCET)[12] and the Asymptomatic Carotid Atherosclerosis Study (ACAS).[13] For patients with conditions matching the criteria for CEA high-risk patients in the Stenting and Angioplasty with Protection in Patients at High Risk for Endarterectomy (SAPPHIRE) study,[14] such as severe heart or lung diseases, over 80 years of age, and occlusion or a high-degree stenosis of the contralateral carotid artery, CAS was chosen rather than CEA. From November 2010, patients >70 years old without other high-risk factors underwent CEA according to the results of the Carotid Revascularization Endarterectomy versus Stenting Trial (CREST) study,[15] which advocated CEA priority for the treatment of elderly patients.

CEA was performed in a standard way with intraluminal shunt and primary closure.[16] CAS was performed using either a PRECISE stent (Cordis, Bridgewater, NJ; 84.7% [50/59]; HCP:LCP 81.2%:86.0%) or a Wallstent (Boston Scientific, Freemont, CA; 15.3% [9/59]; HCP:LCP 14.0%:18.8%) with predilation (6 atm, 30 sec; Sterling, Boston Scientific) and postdilation (10 atm, 10-15 sec; Aviator, Cordis). The same balloon catheters were used for both HCP and LCP groups. Either filter (Angioguard XP; Cordis), distal balloon (PercuSurge Guardwire; Medtronic, Santa Rosa, CA), and/or flow reversal (Patlive; Terumo Clinical Supply, Kakamigahara, Japan) embolic protection devices were used. Aspirin (100 mg/day) was administered before CEA/CAS, and clopidogrel (75 mg/day or cilostazol 200 mg/day) was also prescribed after CAS.

The rates of any type of stroke (including contralateral stroke) and death (including death from causes other than stroke) at 30 days and 6 months were evaluated.

The ethics guidelines for clinical studies issued by the Japanese Health Labor and Welfare Ministry (2008) were strictly observed, while informed patient consent was not required for this retrospective study.

Assessment of Calcification with MDCTA

MDCTA was performed pre- and postoperatively in all patients with a 16-row system (IDT-16; Philips, Amsterdam, the Netherlands). Evaluation of calcification of the plaques using the Agatston calcium score was performed as described.[7] Briefly, calcification of the carotid plaque was quantified using the specialized software implemented in the workstation (Aquarious; TeraRecon Inc,

Table 1. *Clinical characteristics of cases in each surgical treatment group*

	Total	CEA	CAS	*P* value
No. of treatments	140	81	59	—
Age, y (±SD)	70.7 ± 6.7	69.3 ± 6.2	72.3 ± 6.8	.01
Male sex, n (%)	118 (84.3)	66 (81.5)	52 (87.5)	.41
Symptomatic case, n (%)	104 (74.3)	61 (75.3)	44 (73.3)	.92
Degree of carotid stenosis, % (±SD)	78.6 ± 12.2	79.7 ± 9.7	77.1 ± 15.0	.59
Contralateral carotid stenosis, % (±SD)	20.7 ± 30.6	18.2 ± 27.6	23.9 ± 34.3	.26
Calcium score	333.0 ± 583.7	339.6 ± 639.8	323.6 ± 501.7	.52

Abbreviations: CAS, carotid artery stenting; CEA, carotid endarterectomy; SD, standard deviation.

San Mateo, CA) with preoperative MDCTA data. Calcium scores were calculated as the products of the areas of calcified lesions and the weighted signal intensity scalars, dependent on the maximal Hounsfield unit (HU) value within the lesion (scalar = 1 if 130-199 HU, 2 if 200-299, 3 if 300-399, and 4 if ≥400). The analysis of the degrees of stenoses before and after the operation was also performed with MDCTA using the NASCET method.[12] The ROC analysis revealed that the optimal cutoff value for the calcium score was 420 for postoperative residual stenosis >25% after CAS (sensitivity 0.750; specificity 0.764; pseudopositive ratio 0.236; Fig 1). On the basis of this ROC analysis, we divided all cases for further assessment into an HCP group with calcium scores ≥420 and an LCP group with calcium scores <420.

Diffusion-weighted Images of Magnetic Resonance Imaging

Magnetic resonance imaging including diffusion-weighted (DW) images was performed to detect newly developed ischemia as a high-intensity spot (HIS) with a 1.5-T imaging system (Gyroscan Integra; Philips) using a single-shot diffusion echo planar imaging (EPI) sequence with the following parameters: TR 2917 ms, TE 83 ms, flip angle 90°, 5.0-mm section thickness, field of view 23.0 cm, number of excitations 1, b value = 0, and 1000 s/mm^2.

Residual Stenosis, Improvement Rate, and Restenosis/In-stent Restenosis

Residual stenosis was also measured using the NASCET method[12] and stenosis of >25% was counted. The improvement rate was calculated as [100 (preoperative degree of stenosis–postoperative degree of stenosis)/preoperative degree of stenosis]. A multiple logistic regression analysis was performed to find independent preoperative predictors of residual stenosis. Six months after the operations, both restenosis after CEA and in-stent restenosis after CAS of >25% were counted. The latter was detected as a low-density defect in the lumen inside the stent wall in any sagittal or axial multiplanar reconstruction (MPR) images of MDCTA.

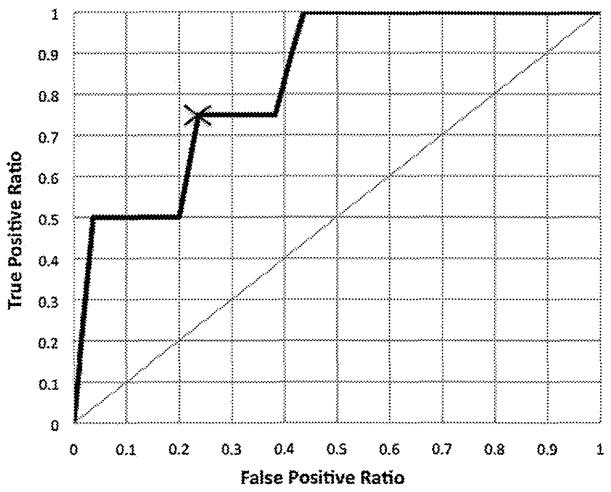

Figure 1. *Receiver operating characteristic (ROC) analysis for the prediction of postoperative residual stenosis of >25% after carotid artery stenting. The optimal cutoff value of the calcium score was revealed to be 420 with a sensitivity of 0.750, specificity of 0.764, pseudopositive ratio of 0.236, and an area under the curve of 0.746.*

Single-photon Emission Computed Tomography and Hyperperfusion

Postoperative N-isopropyl-p-[^{123}I]- iodoamphetamine (IMP)–single-photon emission computed tomography was performed using the autoradiography (ARG) method and checked for the occurrence of hyperperfusion using a dual-head gamma camera system (E.CAM; Siemens, Erlangen, Germany) equipped with high-resolution fan-beam collimators. For data acquisition, we used a 128 × 128 matrix for 36 steps of 5°, field of view 422 mm, and 5-mm slice thickness. Postoperative hyperperfusion was defined as a regional cerebral blood flow (rCBF) increase of >100%[17] compared to the preoperative values in >1 region of interest (ROI) analyzed with a 3-dimensional stereotactic ROI template (3DSRT; Fuji Film RI Pharma Co, Tokyo, Japan).[18,19] Cerebral hyperperfusion syndrome (CHS) was defined as having symptoms such as seizure, deterioration of consciousness level, focal neurologic signs with or without postoperative intracerebral hemorrhage (ICH), and no evidence of new postoperative ischemia.

Statistical Analysis

All statistical evaluations were performed with Statview (version 5.0; SAS Inc, Cary, NC) and StatMate III software (ATMS; Tokyo), and all results are presented as mean ± standard deviation. The ROC analysis was performed to set the cutoff value of the calcium scores in the prediction of residual stenosis after CAS. The Chi-square test with the Yates correction and the Mann–Whitney *U* test were used for comparison. For the multivariate analysis, a logistic regression model was used. $P < .05$ was considered statistically significant.

Results

The characteristics for all cases are shown in Table 1. There were no significant differences between the CEA and CAS groups concerning gender, degree of stenosis, and the percentage of symptomatic cases and calcium scores, except for a slight difference in the mean ages of the groups because of the application of the surgical indication of the SAPPHIRE study.[14]

The HCP group consisted of 20 (24.7%) CEA cases and 16 (27.1%) CAS cases (Table 2). The mean residual degree

Table 2. *Comparison of the results for carotid endarterectomy and carotid artery stenting with regard to plaque calcification*

Plaque calcification	Total	CEA				CAS			
		All	Low	High	*P* value*	All	Low	High	*P* value†
No. of treatments, n (%)	140	81	61 (75.3)	20 (24.7)	—	59	43 (72.9)	16 (27.1)	—
Mean calcium score, n (±SD)	333.0 ± 583.7	339.6 ± 639.8	107.3 ± 127.7	1048.1 ± 985.1	—	323.6 ± 501.7	121.0 ± 132.0	867.8 ± 700.6	—
Mean residual stenosis, % (±SD)	4.6 ± 13.9	5.1 ± 16.6	4.3 ± 13.8	6.8 ± 22.7	.60	4.3 ± 9.5	1.7 ± 6.1	9.7 ± 13.3	<.001‡
Improvement rate, % (±SD)	94.5 ± 16.0	93.8 ± 18.8	94.6 ± 16.4	92.4 ± 24.2	.59	94.8 ± 12.1	97.9 ± 7.9	87.0 ± 16.8	<.001‡
High intensity spots on DW MRI, % (n)	23.3 (24/103)	22.6 (12/53)	24.4 (10/41)	16.7 (2/12)	.57	24.0 (12/50)	20.0 (7/35)	33.3 (5/15)	.52
Restenosis/In-stent restenosis,‡n (%)	15 (10.7)	8 (9.9)	4 (6.6)	4 (20.0)	.08	7 (11.9)	4 (9.3)	3 (18.8)	.59
Cerebral hyperperfusion syndrome, n (%)	2 (1.4)	0 (0)	0 (0)	0 (0)	—	2 (3.4)	1 (2.3)	1 (6.3)	.95
Cranial nerve palsy, n (%)	4 (2.9)	4 (4.9)	4 (6.6)	0 (0)	—	0 (0)	0 (0)	0 (0)	—
30-day stroke or death rate, (%)	4 (2.9)	1 (1.2)	1 (1.6)§	0 (0)	—	3 (5.1)	1 (2.3)	2 (12.5)	.36
6-month stroke or death rate, n (%)	4 (2.9)	1 (1.2)	1 (1.6)§	0 (0)	—	3 (5.1)	1 (2.3)	2 (12.5)	.36

Abbreviations: CAS, carotid artery stenting; CEA, carotid endarterectomy; DW, diffusion-weighted; MRI, magnetic resonance imaging; SD, standard deviation.
*Comparison between carotid stenoses with low- and high-calcified plaques treated by CEA.
†Comparison between carotid stenoses with low- and high-calcified plaques treated by CAS.
‡Restenosis >25%.
§A case with contralateral stroke.

of stenosis after CAS for the HCP group was 9.7% ± 13.3%, whereas that for the LCP group was 1.7% ± 6.1% ($P < .001$). In comparison, the mean residual degree of stenosis after CEA for the HCP group was 6.8% ± 22.7%, whereas that for the LCP group was 4.3% ± 13.8%. The postoperative mean improvement rates of stenosis for the HCP group were 92.4% ± 24.2% in the CEA cases and 87.0% ± 16.8% in the CAS cases, whereas those for the LCP group were 94.6% ± 16.4% and 97.9% ± 7.9%, respectively. Representative cases of the HCP group for CEA and CAS were shown in Figures 2 and 3. Multiple logistic regression analysis revealed that only the calcium score was an independent pre-CAS predictor of residual stenosis (Table 3). Immediate occlusion of carotid artery was observed in 2 cases after CEA without any stroke or symptoms (1 case each in the LCP and HCP groups).

Postoperative DW images of magnetic resonance imaging (MRI) were obtained in 73.6% of all cases and revealed HIS in 16.7% and 33.3% of the HCP group after CEA and CAS, respectively, but in 24.4% and 20.0%, respectively, in the LCP group.

At 6 months after CEA, restenoses >25% were observed in a total of 8 patients (9.9%; 4 in each group; 6.6% and 20% for LCP and HCP, respectively). Stenosis was ameliorated after 1 year in 1 patient, and no remarkable deterioration in the degree of stenosis without clinical symptoms was observed in 3 patients. The other 4 patients were treated by CAS after 9 to 13 months. In-stent restenosis (>25%) 6 months after CAS was found in 4 (9.3%) and 3 cases (18.8%) in the LCP and HCP groups, respectively. CHS was observed in 2 cases of CAS, 1 in each group. The 30-day and 6-month rates for any stroke or death after CEA were both 1.2% in the LCP group (for a 66-year-old contralateral internal carotid occlusion patient who suffered a contralateral parietal stroke) and 0% in the HCP group. Postoperative cranial nerve palsy was seen in 4 carotid stenoses with LCP after CEA, half as hoarseness and the rest as facial nerve palsy, although the symptoms were transient. The 30-day and 6-month rates for any stroke or death after CAS were 2.3% and 12.5% for both LCP and HCP, because of a postoperative fatal ICH of a 74-year-old man in the LCP group, an ipsilateral stroke of an 84-year-old woman, and CHS of an 80-year-old woman in the HCP group.

Discussion

In the present study, the mean degrees of residual stenosis after CAS were apparently greater in patients with carotid stenoses with calcified plaques that had a calcium score >420 compared to the less calcified plaques, whereas the mean degrees of residual stenosis after CEA showed no significant difference between the 2 patient groups. McCabe et al[20] reported that poor initial dilation of the lesion was responsible for 38% of the endovascular patients in the Carotid and Vertebral Artery

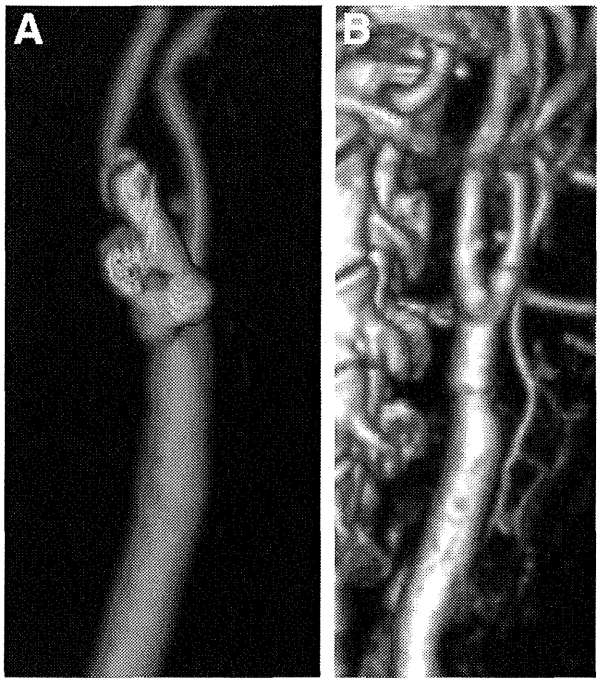

Figure 2. *A right carotid endarterectomy case of a 76-year-old woman with 75% carotid stenosis. (A) Preoperative computed tomographic angiography revealed a high-calcified plaque at the right carotid bifurcation (calcium score 625.9). (B) Postoperative computed tomographic angiography revealed excellent dilatation with disappearance of calcification.*

Transluminal Angioplasty Study (CAVATAS) who were found to have severe stenosis at 1 year. In addition, Aronow et al[21] observed that there was a greater risk of neurologic death or stroke after CAS when the final residual diameter stenosis was >30%, and Randall et al[22] also pointed out the importance of residual stenosis >50% as a possible risk factor for recurrent stroke events.

To counterbalance the external pressure created by severe calcification and to obtain satisfactory stent expansion, additional dilatation plus the original radial force of a self-expanding stent seems essential through postdilation with a balloon catheter. However, hypotension and bradycardia from the stretching of the carotid sinus baroreceptor after CAS are known to be influenced by the magnitude of the dilation performed,[23] and moreover, several reports[10,11] also indicated that the presence of calcification in plaque was significantly related with increased rate of stent fracture or deformation. Expansion of the stent was therefore occasionally reduced, especially in severe carotid stenosis. We calculated the improvement rate of stenosis in the present study. The mean improvement rate of the HCP group was, however, lower than that of the LCP group after CAS (87.0% ± 16.8% *v* 97.9% ± 7.9%), whereas CEA had good improvement rates regardless of calcification in plaques.

The reason that residual stenosis after CAS for the LCP group was even less than that of the CEA group in our study is not apparent. The percentage using the Wallstent was not significantly different (18.8% for HCP and 14.0% for LCP), and the same balloon catheters were used for both groups. We strictly counted transient dents made by tourniquets used in CEA as residual stenosis that could be usually restored in a year, which might lead to a relatively higher degree of residual stenosis in CEA.

It was reported in 2008 that the total volume of calcification in carotid plaques did not correlate with residual stenosis,[24] and the study's authors concluded that CAS using embolic protection devices was feasible even in patients with near-total circumferential plaque calcification. They also reported that fragmentations of the calcifications were confirmed in 17 of 18 plaques with a mean arc of calcification ranging from 278° to 360°.[25] However, in these studies, the plaque calcification volume was determined by manual tracing on computed tomographic sections, without an assessment of the hardness of the calcification, and the results were not compared with those after CEA. From the results of the present study, it might be important to analyze calcified plaques using calcium scores for precise assessment of calcification

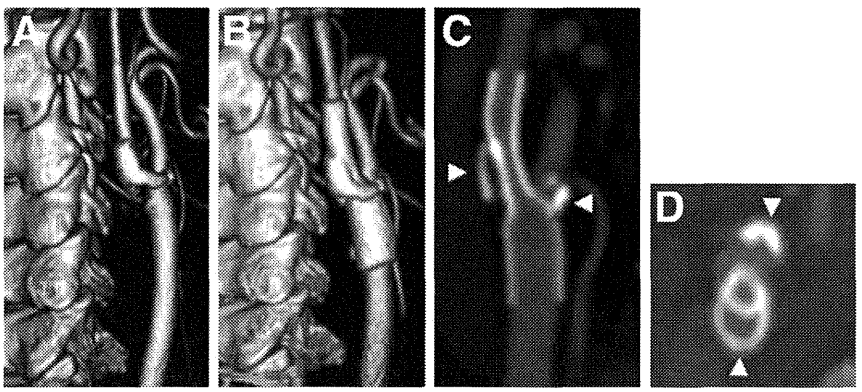

Figure 3. *A right carotid artery stenting case of a 77-year-old man with 90% carotid stenosis. (A) Preoperative computed tomography angiography (CTA) revealed a high-calcified plaque at the right carotid bifurcation (calcium score 1076.8). (B) Carotid artery stenting was performed using a PRECISE stent (Cordis, Bridgewater, NJ) with predilation (6 atm, 30 sec) and postdilation (10 atm, 15 sec) by balloon catheters and a PercuSurge Guardwire (Medtronic, Santa Rosa, CA) distal balloon embolic protection device. Postoperative CTA revealed calcification outside the stent, as it was preoperatively. (C) A sagittal multiplanar reconstruction image of the postoperative CTA scan revealed 27.6% residual stenosis with calcification outside the stent* (arrowheads). *(D) An axial multiplanar reconstruction image of the postoperative CTA scan also revealed restriction in the stent expansion from calcification* (arrowheads).

Table 3. *Multiple logistic regression analysis for residual stenosis after carotid artery stenting with preoperative factors*

	OR	95% CI	*P* value
Age	0.65	0.10-4.26	.65
Male sex	0.42	0.04-4.49	.47
Symptomatic case	0.49	0.07-3.25	.46
Ipsilateral high-grade carotid stenosis	0.53	0.06-5.11	.58
Contralateral carotid stenosis	3.06	0.27-34.34	.36
Calcium score	13.67	1.39-134.20	.025*
Hypertension	2.84	0.30-27.17	.37
Diabetes mellitus	3.47	0.53-22.80	.20

Abbreviations: CI, confidence interval; OR, odds ratio.
*Denotes statistical significance.

including hardness and conventional morphologic evaluation.

A systemic review of the literature revealed that the incidence of new lesions was significantly higher after CAS (37%) than after CEA (10%).[26] In our series, detection rates of new HIS on DW images of MRI for HCP were higher after CAS and lower after CEA than those for LCP, although they were not significant. The reason for this result is not clear, but the relatively low mean calcium scores for HCP in CAS compared to those in CEA, which suggested that relatively more components other than hard calcification were contained, might have contributed to this difference. The smaller percentage of screened DW images of MRI for CEA compared to CAS (65.4% *v* 84.7%) might have also affected our results.

Watarai et al[27] reported that in-stent hypodense areas after CAS were found in 43.5% of their cases. In the present study, the total detection rate was 11.9% and in-stent thrombosis/restenosis was observed more frequently in the patients with HCP, although it was not significant. In the Endarterectomy Versus Angioplasty in Patients with Symptomatic Severe Carotid Stenosis (EVA-3S) study,[28] the rate of restenosis >50% after CEA was reported to be 5.0%, which was less than half of that after CAS (12.5%). Considering that the reported frequency of restenosis after CEA (mostly stenosis >50%) ranges from 7.5% to 17%,[29-31] our data (9.9%) might be comparable to the previous study, although we extracted restenosis >25%, applying the same criteria as in the assessment of residual stenosis. The rate of restenosis after CEA might be reduced by applying a patch instead of doing primary closure.[32] In our study, restenosis was detected more often in cases with HCP than in those with LCP, although it was not significant, as with CAS. This is in line with the previous report by Hellings et al,[30] who found that lipid-rich, inflammatory plaques were associated with a reduced risk of restenosis.

In the present study, 2 cases of CHS after CAS were encountered, 1 each in the LCP and HCP groups. Risk factors for CHS have been reported, including severe ipsilateral stenosis >90%, low cerebrovascular reserve, impaired collateral blood flow, and perioperative hypertension.[33,34] In the present study, hardness or the character of the plaques seemed to be scarcely related to the occurrence of CHS.

The 30-day and 6-month rates for any stroke or death in the present study were both higher for CAS than CEA because of the 2 cases of CHS and 1 case of ipsilateral stroke just after the procedure, although no significant difference was found between the LCP and HCP groups. The rates of periprocedural death or any stroke for CEA/CAS were comparable to those reported to be 3.2% and 6.0% in the CREST study[15] and 3.8% and 9.4% in the EVA-3S study,[35] respectively.

The main limitations of our study are the relatively small sample size and the short follow-up period. Additional studies with larger numbers of patients and longer follow-up are warranted to clarify the issue.

In conclusion, treatment by CAS for carotid stenoses with HCP may lead to more residual stenosis than CAS for carotid stenoses with LCP, and may in turn elicit a subsequent stroke or unfavorable events. From the results of the present study, it may be reasonable to choose CEA as an alternative treatment to reduce residual stenosis and the possibility of critical events for the treatment of carotid stenoses with calcified plaque with a calcium score ≥420. To determine what treatment is appropriate for carotid stenoses with calcified plaques, it might be important to evaluate calcification not only by traditional morphologic assessment whether it is near-circumferential or not, but also by quantity (volume) and quality (hardness) using calcium scores.

Acknowledgment: We are grateful to Dr. Noritaka Aihara and our all ward staff for their invaluable clinical contributions.

References

1. Hayashi K, Kitagawa N, Morikawa M, et al. Case of internal carotid artery stenosis complicated with shower embolism during filter-protected carotid artery stenting [in Japanese]. Brain Nerve 2009;61:83-87.
2. Sorimachi T, Nishino K, Morita K, et al. Flow impairment during filter-protected carotid artery stent placement: Frame-by-frame evaluation of digital subtraction angiography images. World Neurosurg 2011;76:282-287.
3. Brewster LP, Beaulieu R, Corriere MA, et al. Carotid revascularization outcomes comparing distal filters, flow reversal, and endarterectomy. J Vasc Surg 2011; 54:1000-1004.
4. Taha MM, Maeda M, Sakaida H, et al. Cerebral ischemic lesions detected with diffusion-weighted magnetic resonance imaging after carotid artery stenting: Comparison

of several anti-embolic protection devices. Neurol Med Chir (Tokyo) 2009;49:386-393.
5. Katano H, Kato K, Umemura A, et al. Perioperative evaluation of carotid endarterectomy by 3D-CT angiography with refined reconstruction: Preliminary experience of CEA without conventional angiography. Br J Neurosurg 2004;18:138-148.
6. Niwa Y, Katano H, Yamada K. Calcification in carotid atheromatous plaque: Delineation by 3D-CT angiography, compared with pathological findings. Neurol Res 2004; 26:778-784.
7. Katano H, Yamada K. Analysis of calcium in carotid plaques with Agatston scores for appropriate selection of surgical intervention. Stroke 2007;38:3040-3044.
8. Nonaka T, Oka S, Miyata K, et al. Prediction of prolonged postprocedural hypotension after carotid artery stenting. Neurosurgery 2005;57:472-477.
9. Tyden G, Samnegard H, Thulin L. Rational treatment of hypotension after carotid endarterectomy by carotid sinus nerve blockade. Acta Chir Scand Suppl 1980; 500:61-64.
10. Chang CK, Huded CP, Nolan BW, et al. Prevalence and clinical significance of stent fracture and deformation following carotid artery stenting. J Vasc Surg 2011; 54:685-690.
11. Coppi G, Moratto R, Veronesi J, et al. Carotid artery stent fracture identification and clinical relevance. J Vasc Surg 2010;51:1397-1405.
12. North American Symptomatic Carotid Endarterectomy Trial Collaborators. Beneficial effect of carotid endarterectomy in symptomatic patients with high-grade carotid stenosis. N Engl J Med 1991;325:445-453.
13. Executive Committee for the Asymptomatic Carotid Atherosclerosis Study. Endarterectomy for asymptomatic carotid artery stenosis. JAMA 1993;273:1421-1428.
14. Yadav JS, Wholey MH, Kunts RE, et al. Stenting and angioplasty with protection in patients at high risk for endarterectomy investigators. Protected carotid-artery stenting versus endarterectomy in high-risk patients. N Engl J Med 2004;351:1453-1501.
15. Brott TG, Hobson RW II, Howard G, et al. Stenting versus endarterectomy for treatment of carotid-artery stenosis. N Engl J Med 2010;363:11-23.
16. Katano H, Yamada K. Carotid endarterectomy for stenoses of twisted carotid bifurcations. World Neurosurgery 2010;73:147-154.
17. Hosoda K, Kawaguchi T, Ishii K, et al. Comparison of conventional region of interest and statistical mapping method in brain single-photon emission computed tomography for prediction of hyperperfusion after carotid endarterectomy. Neurosurgery 2005;57:32-41.
18. Takeuchi R, Sengoku T, Matsumura K. Usefulness of fully automated constant ROI analysis software for the brain: 3DSRT and FineSRT. Radiat Med 2006; 24:538-544.
19. Torigai T, Mase M, Ohno T, et al. Usefulness of dual and fully automated measurements of cerebral blood flow during balloon occlusion test of the internal carotid artery. J Stroke Cerebrovasc Dis 2013;22:197-204.
20. McCabe DJH, Pereira AC, Clifton A, et al. Restenosis after carotid angioplasty, stenting, or endarterectomy in the Carotid and Vertebral Artery Transluminal Angioplasty Study (CAVATAS). Stroke 2005;36:281-286.
21. Aronow HD, Gray WA, Ramee SR, et al. Predictors of neurological events associated with carotid artery stenting in high-surgical-risk patients. Insights from the Cordis Carotid Stent Collaborative. Circ Cardiovasc Interv 2010;3:577-584.
22. Randall MS, McKevitt FM, Kumar S, et al. Long-term results of carotid artery stents to manage symptomatic carotid artery stenosis and factors that affect outcome. Circ Cardiovasc Interv 2010;3:50-56.
23. Lavoie P, Rutledge J, Dawoud MA, et al. Predictors and timing of hypotension and bradycardia after carotid artery stenting. AJNR Am J Neuroradiol 2008;29:1942-1947.
24. Tsutsumi M, Aikawa H, Onizuka M, et al. Carotid artery stenting for calcified lesions. AJNR Am J Neuroradiol 2008;29:1590-1593.
25. Tsutsumi M, Kodama T, Aikawa H, et al. Fragmentation of calcified plaque after carotid artery stenting in heavily calcified circumferential stenosis. Neuroradiology 2010; 52:831-836.
26. Schnaudigel S, Gröschel K, Pilgram SM, et al. New brain lesions after carotid stenting versus carotid endarterectomy. A systematic review of the literature. Stroke 2008; 39:1911-1919.
27. Watarai H, Kaku Y, Yamada M, et al. Follow-up study on in-stent thrombosis after carotid stenting using multidetector CT angiography. Neuroradiology 2009;51:243-251.
28. Mas JL, Chatellier G, Beyssen B. Carotid angioplasty and stenting with and without cerebral protection: Clinical alert from the Endarterectomy Versus Angioplasty in Patients With Symptomatic Severe Carotid Stenosis (EVA-3S) trial. Stroke 2004;35:e18-e21.
29. Goodney PP, Nolan BW, Eldrup-Jorqensen J, et al. Vascular study group of Northern New England: Restenosis after carotid endarterectomy in a multicenter regional registry. J Vasc Surg 2010;52:897-905.
30. Hellings WE, Moll FL, De Vries JP, et al. Atherosclerotic plaque composition and occurrence of restenosis after carotid endarterectomy. JAMA 2008;299:547-554.
31. Makihara N, Toyoda K, Uda K, et al. Characteristic sonographic findings of early restenosis after carotid endarterectomy. J Ultrasound Med 2008;27:1345-1352.
32. Mannheim D, Weller B, Vahadim E, et al. Carotid endarterectomy with a polyurethane patch versus primary closure: A prospective randomized study. J Vasc Surg 2005; 41:403-408.
33. Kaku Y, Yoshimura S, Kokuzawa J. Factors predictive of cerebral hyperperfusion after carotid angioplasty and stent placement. AJNR Am J Neuroradiol 2004; 25:1403-1408.
34. van Mook WNKA, Rennenberg RJMW, Schurink GW, et al. Cerebral hyperperfusion syndrome. Lancet Neurol 2005;4:877-888.
35. Arquizan C, Trinquart L, Touboul PJ, et al. Restenosis is more frequent after carotid stenting than after endarterectomy: The EVA-3S Study. Stroke 2011;42:1015-1020.

Upregulation of ANGPTL4 Messenger RNA and Protein in Severely Calcified Carotid Plaques

Hiroyuki Katano, MD, PhD,*† and Kazuo Yamada, MD, PhD*

Background: In carotid atherosclerotic lesions, calcified plaques are thought to be stable and to evoke very few symptoms. However, the molecular activity in calcified plaques and their clinical significance have not been fully clarified yet. *Methods:* Carotid plaques from 18 endarterectomy patients were classified into high- and low-calcified plaques on the basis of Agatston calcium score. Twelve plaques were investigated for the alteration of gene expression by microarray analysis and real-time polymerase chain reaction (PCR) and 6 other plaques underwent protein assessment to elucidate the difference in molecular biological activity between the groups. *Results:* Microarray analysis demonstrated 93 angiogenesis or growth factor–related transcripts that are reliably expressed (175 probe sets). Among them, angiopoietin-like protein 4 (ANGPTL4) expression was significantly elevated, whereas fibroblast growth factor receptor 2 (FGFR2) expression was significantly suppressed. Quantitative messenger RNA analysis was performed with real-time PCR. Augmented or decreased protein expression of each gene was confirmed by Western blotting analysis and immunohistochemistry. *Conclusions:* In high-calcified plaques, ANGPTL4 might be upregulated for antiangiogenic modulating function together with the downregulation of FGFR2, contributing to the stability of the plaques. **Key Words:** Carotid plaque—calcification—microarray analysis—ANGPTL4—FGFR2—angiogenesis.

Introduction

The mechanism of vascular calcification formation and its clinical significance have not been fully clarified yet. Calcification has been thought to be a terminal state of the tissue in the pathological course of atherosclerosis that ended up in necrosis or apoptosis. Apoptotic bodies derived from vascular smooth muscle cells have been reported to serve as a nidus for calcification.[1] Lipoprotein such as acetylated low-density lipoprotein in atherosclerotic plaque was found to prevent phagocytosis of vascular-derived apoptotic vesicles that would otherwise serve as a core of calcification.[2] In carotid atherosclerotic lesions, calcified plaques were, hence, thought to be stable and hardly evoke symptoms, whereas unstable deleterious plaques were reported to be so-called "soft," hemorrhagic, or mobile plaques.[3] Nandalur et al[4] reported that plaque calcification of more than 45% of the total volume was significantly inversely associated with the occurrence of symptoms, whereas Kwee[5] found through a systematic review that clinically symptomatic plaques have a lower degree of calcification than asymptomatic plaques.

We planned, therefore, to classify the carotid plaques into high- and low-calcified plaques on the basis of

From the *Department of Neurosurgery, Nagoya City University Graduate School of Medical Sciences, Nagoya; and †Department of Medical informatics and Integrative Medicine, Nagoya City University Graduate School of Medical Sciences, Nagoya, Japan.

Received April 3, 2013; revision received July 27, 2013; accepted July 31, 2013.

Funding: This work was supported by JSPS KAKENHI (grant number 23592102).

Conflict of interests: The authors declared no conflicts of interest with respect to the authorship and/or publication of this article.

Address correspondence to Hiroyuki Katano, MD, PhD, Department of Neurosurgery, Nagoya City University Graduate School of Medical Sciences, 1 Kawasumi, Mizuho-cho, Mizuho-ku, Nagoya 467-8601, Japan. E-mail: katano@med.nagoya-cu.ac.jp.

1052-3057/$ - see front matter

http://dx.doi.org/10.1016/j.jstrokecerebrovasdis.2013.07.046

Agatston calcium score and investigate the alteration of gene expression by microarray analysis followed by protein assessment to elucidate the difference in molecular biological activity between the groups.

Materials and Methods

Patients and Specimens

Carotid plaques from 18 endarterectomy patients were investigated. Of these, 12 plaques were used for the gene expression analysis and another 6 plaques were used for Western blotting and immunohistochemistry. In each group, half of the plaques were highly calcified plaques that showed a mean calcium score of 839.9 ± 569.0, whereas the rest of the low-calcified plaques showed a mean calcium score of 52.5 ± 36.7. Macroscopic hemorrhages and ulcers were more frequently found in the low-calcified plaques than the high-calcified ones. The percentage of symptomatic cases was the same (77.8%) in both groups, and there were no significant differences in the degrees of stenoses between the groups (83.8% ± 11.0% versus 80.6% ± 6.2%). No remarkable difference was found between high- and low-calcified plaques concerning clinical data except hypertension and smoking habit (Table 1).

All patients enrolled in this study received a detailed explanation on the nature of the project, and all gave written informed consent before undergoing endarterectomy. Approval of the local ethical committee for human genetic research was also obtained before the start of the study. The patients underwent preoperative multidetector computed tomography angiography (MDCTA) that identified the plaque location and the degree of stenosis. Evaluation of calcification of the plaques using Agatston calcium score was also performed using MDCTA as described previously.[6] Briefly, calcification of the carotid plaque was quantified using specialized software run on the workstation (Aquarious; TeraRecon, Inc., San Mateo, CA) with preoperative MDCTA data. Calcium scores were calculated as the products of the areas of calcified lesions and the weighted signal intensity scalars, dependent on the maximal Hounsfield unit value within the lesion (scalar = 1 if 130-199, 2 if 200-299, 3 if 300-399, and 4 if 400 Hounsfield units or greater). All carotid plaques were obtained during carotid endarterectomy, and whole specimens containing a calcified portion were immediately treated with RNA later (Ambion, Austin, TX). All samples were stored at −80°C and thawed only once.

Microarray

The methods used for sample preparation, hybridization, data analysis, sensitivity, and quantification are based on the Affymetrix GeneChip Expression Analysis Manual (Affymetrix, Santa Clara, CA). We used Affymetrix Human Genome U133 Plus 2.0 Array containing more than 54,000 probe sets representing 47,400 transcripts derived from 38,500 well-substantiated human genes and expressed sequence tags (unknown genes).

Total RNA was extracted from each plaque sample, cleaned, and converted to double-stranded complementary DNA (cDNA) and then to biotin-labeled complementary RNA according to the manufacturer's protocols. After quality confirmation with an Agilent 2100 Bioanalyzer (Aligent Technologies, Santa Clara, CA), biotinylated complementary RNA was hybridized to the Affymetrix Human Genome U133 Plus 2.0 chips. Hybridization of each chip was performed with the Hybridization, Wash, and Stain Kit according to GeneChip 3'IVT Express Kit User Manual and scanned with a probe array scanner. GeneChip raw data were obtained with Affymetrix GeneChip Command Console Software. After the mean value for the signal of each chip was normalized and scaled using the Micro Array Suite 5 statistical algorithm with Affymetrix Expression Console Software, analysis of the expression ratio comparing low and highly calcified groups was performed. Processed gene expression data were returned in a log2 scale. We compared 7 sets of high- and low-calcified plaques: set A: H1/L1, B: H2/L1, C: H3/L1, D: H1/L2, E: H2/L2, F: H3/L2, and G: H1/L3. Genes expressed at a reliable level and showing differential expression were identified by filtering. Detection calls were classified as present (P; transcripts detected), absent (A; transcripts not detected), or marginal (M; difficult to judge whether P or A). A transcript was considered differentially expressed if it satisfied the either following criteria: (1) (log2 ratio ≥ 1 and the detection call of the highly calcified plaque "P") in more than 5 of 7 comparison sets or (2) (log2 ratio ≤ -1 and the detection call of the low-calcified plaque "P") in more than 5 of 7 comparison sets. Among all the expressed transcripts by GeneChip analysis, angiogenesis or growth factor–related, calcification or osteogenesis-related and hypoxia-inducible transcripts were focused to extract for further analysis.

Real-Time Polymerase Chain Reaction

Three high-calcified plaques (H4: 797.6, H5: 995.5, H6: 2244.2) and 3 low-calcified plaques (L4: 2.0, L5: 4.8, L6: 95.0) were used for real-time polymerase chain reaction (PCR) analysis for angiogenesis or growth factor–related transcripts expressed differently by microarray analysis. Five hundred nanograms of total RNA from each sample was reverse transcribed with oligodT and random hexamer primers using Transcriptor First Strand cDNA Synthesis Kit (Roche Diagnostics, Basel, Switzerland). Twenty microliters reactions containing 3 μL cDNA and gene-specific primers were added to SYBRGreen I Master

Table 1. *Characteristics of the plaques and the clinical data*

Plaque	Ca score	Hemorrhage	Ulcer	Age	Gender	Stenosis (%)	Symptom	Hypertension	Diabetes	Dyslipidemia	Smoking	Antiplatelet	Anticoagulant	Renal malfunction
H1	558.4	+	−	73	M	83.0	A	+	+	+	+	+	−	−
H2	323.7	−	−	63	M	90.0	S	+	−	+	+	+	−	−
H3	434.0	−	−	70	M	85.0	A	+	−	−	+	+	−	−
H4	797.6	+	−	70	M	80.0	S	+	−	+	+	+	−	−
H5	995.5	−	−	65	M	95.0	S	+	−	+	+	+	−	−
H6	2244.2	−	−	70	M	76.5	S	−	−	+	+	+	−	−
H7	911.1	−	−	74	F	60.0	S	+	−	−	−	+	−	−
H8	680.9	−	−	66	F	90.0	S	+	−	+	+	+	−	−
H9	614.0	−	−	63	M	95.0	S	−	+	−	+	+	−	−
L1	38.8	+	−	67	M	80.0	S	+	+	+	−	+	−	−
L2	68.3	−	−	67	M	78.0	A	−	−	−	−	+	−	−
L3	98.0	+	+	74	F	90.0	S	+	−	−	+	+	−	−
L4	2.0	+	+	73	M	81.5	S	−	−	+	+	+	−	−
L5	4.8	+	+	66	M	73.0	S	+	+	+	+	+	−	−
L6	95.0	−	−	76	M	90.0	S	+	−	−	+	+	−	−
L7	26.6	+	−	68	M	75.0	S	−	−	+	−	+	−	−
L8	55.5	+	+	60	M	83.0	A	−	+	+	+	+	−	−
L9	83.5	−	−	74	M	75.0	S	+	−	−	+	+	+	−

Abbreviations: A, asymptomatic; F, female; M, male; H1-H9, high-calcified plaques; L1-L9, low-calcified plaques; S, symptomatic.

Table 2. *All angiogenesis and growth factor–related transcripts detected in microarray analysis for high- and low-calcified carotid plaques*

No.	Probe set ID	Probe ID	Representative public ID	Gene symbol	Gene title	Average log2 ratio
1	213176_s_at	HU133p2_22479	AI910869	LTBP4	Latent transforming growth factor beta binding protein 4	1.73
2	204200_s_at	HU133p2_13648	NM_002608	PDGFB	Platelet-derived growth factor beta polypeptide (simian sarcoma viral (v-sis) oncogene homolog)	1.24
3	201508_at	HU133p2_10957	NM_001552	IGFBP4	Insulin-like growth factor–binding protein 4	1.22
4	223333_s_at	HU133p2_32611	AF169312	ANGPTL4*	Angiopoietin-like protein 4	1.17
5	231762_at	HU133p2_41017	NM_004465	FGF10	Fibroblast growth factor 10	1.12
6	207334_s_at	HU133p2_16779	NM_003242	TGFBR2	Transforming growth factor, beta receptor II (70/80 kDa)	1.08
7	220789_s_at	HU133p2_30074	NM_004749	TBRG4	Transforming growth factor beta regulator 4	1.08
8	223836_at	HU133p2_33113	AB021123	FGFBP2	Fibroblast growth factor–binding protein 2	1.04
9	207822_at	HU133p2_17262	NM_023107	FGFR1	Fibroblast growth factor receptor 1	1.04
10	1555997_s_at	HU133p2_02723	BM128432	IGFBP5	Insulin-like growth factor–binding protein 5	.97
11	209908_s_at	HU133p2_19315	BF061658	TGFB2	Transforming growth factor, beta 2	.93
12	203425_s_at	HU133p2_12873	NM_000599	IGFBP5	Insulin-like growth factor–binding protein 5	.92
13	216061_x_at	HU133p2_25354	AU150748	PDGFB	Platelet-derived growth factor beta polypeptide (simian sarcoma viral (v-sis) oncogene homolog)	.90
14	221009_s_at	HU133p2_30294	NM_016109	ANGPTL4	Angiopoietin-like protein 4	.90
15	204442_x_at	HU133p2_13890	NM_003573	LTBP4	Latent transforming growth factor beta binding protein 4	.81
16	203424_s_at	HU133p2_12872	AW157548	IGFBP5	Insulin-like growth factor–binding protein 5	.76
17	211513_s_at	HU133p2_20840	AF172449	OGFR	Opioid growth factor receptor	.71
18	210973_s_at	HU133p2_20341	M63889	FGFR1	Fibroblast growth factor receptor 1	.70
19	227760_at	HU133p2_37015	AL522781	IGFBPL1	Insulin-like growth factor–binding protein-like 1	.69
20	223321_s_at	HU133p2_32599	AF312678	FGFRL1	Fibroblast growth factor receptor-like 1	.69
21	1561365_at	HU133p2_05958	AA609131	NRP1	Vascular endothelial cell growth factor 165 receptor/neuropilin (VEGF165)	.67
22	1552721_a_at	HU133p2_00329	NM_033136	FGF1	Fibroblast growth factor 1 (acidic)	.67
23	1552939_at	HU133p2_00488	NM_139290	ANGPT1	Angiopoietin 1	.67
24	210628_x_at	HU133p2_20014	AF051344	LTBP4	Latent transforming growth factor beta binding protein 4	.65
25	209542_x_at	HU133p2_18956	M29644	IGF1	Insulin-like growth factor 1 (somatomedin C)	.64
26	210998_s_at	HU133p2_20366	M77227	HGF	Hepatocyte growth factor (hepapoietin A; scatter factor)	.64
27	219922_s_at	HU133p2_29207	NM_021070	LTBP3	Latent transforming growth factor beta binding protein 3	.63
28	243799_x_at	HU133p2_53050	T40942	ANGPTL3	Angiopoietin-like 3, mRNA (cDNA clone IMAGE:3934961)	.61
29	202718_at	HU133p2_12167	NM_000597	IGFBP2	Insulin-like growth factor–binding protein 2, 36 kDa	.61
30	203683_s_at	HU133p2_13131	NM_003377	VEGFB	Vascular endothelial growth factor B	.60
31	205117_at	HU133p2_14565	X59065	FGF1	Fibroblast growth factor 1 (acidic)	.60
32	220961_s_at	HU133p2_30246	NM_030900	TBRG4	Transforming growth factor beta regulator 4	.59
33	201506_at	HU133p2_10955	NM_000358	TGFBI	Transforming growth factor, beta-induced, 68 kDa	.58
34	211958_at	HU133p2_21266	R73554	IGFBP5	Insulin-like growth factor–binding protein 5	.56
35	202273_at	HU133p2_11722	NM_002609	PDGFRB	Platelet-derived growth factor receptor, beta polypeptide	.56
36	204731_at	HU133p2_14179	NM_003243	TGFBR3	Transforming growth factor, beta receptor III	.56

37	205608_s_at	HU133p2_15056	U83508	ANGPT1	Angiopoietin 1	.55
38	237261_at	HU133p2_46511	BE501356	ANGPT2	Angiopoietin 2	.55
39	213910_at	HU133p2_23210	AW770896	IGFBP7	Insulin-like growth factor–binding protein 7	.54
40	210443_x_at	HU133p2_19842	AF172452	OGFR	Opioid growth factor receptor	.54
41	201984_s_at	HU133p2_11433	NM_005228	EGFR	Epidermal growth factor receptor (erythroblastic leukemia viral (v-erb-b) oncogene homolog, avian)	.53
42	206814_at	HU133p2_16261	NM_002506	NGF	Nerve growth factor (beta polypeptide)	.52
43	235277_at	HU133p2_44527	BG334930	AMOTL1	Angiomotin-like 1	.52
44	203085_s_at	HU133p2_12535	BC000125	TGFB1	Transforming growth factor, beta 1	.51
45	226625_at	HU133p2_35881	AW193698	TGFBR3	Transforming growth factor, beta receptor III	.51
46	203851_at	HU133p2_13299	NM_002178	IGFBP6	Insulin-like growth factor–binding protein 6	.51
47	242701_at	HU133p2_51951	AW977978	TBRG1	Transforming growth factor beta regulator 1	.50
48	201983_s_at	HU133p2_11432	AW157070	EGFR	Epidermal growth factor receptor (erythroblastic leukemia viral (v-erb-b) oncogene homolog, avian)	.50
49	207501_s_at	HU133p2_16944	NM_004113	FGF12	Fibroblast growth factor 12	.48
50	209540_at	HU133p2_18954	AU144912	IGF1	Insulin-like growth factor 1 (somatomedin C)	.47
51	212143_s_at	HU133p2_21450	BF340228	IGFBP3	Insulin-like growth factor–binding protein 3	.47
52	205210_at	HU133p2_14658	NM_004257	TGFBRAP1	Transforming growth factor, beta receptor associated protein 1	.46
53	1557285_at	HU133p2_03547	AI891075	AREGB	PREDICTED: *Homo sapiens* similar to amphiregulin precursor, mRNA	.46
54	231382_at	HU133p2_40637	AI798863	FGF18	Fibroblast growth factor 18, mRNA (cDNA clone MGC: 10529 IMAGE: 3948893)	.45
55	211599_x_at	HU133p2_20925	U19348	MET	Met proto-oncogene (hepatocyte growth factor receptor)	.44
56	210764_s_at	HU133p2_20146	AF003114	CYR61	Cysteine-rich, angiogenic inducer, 61	.43
57	211527_x_at	HU133p2_20854	M27281	VEGFA	Vascular endothelial growth factor A	.43
58	211148_s_at	HU133p2_20512	AF187858	ANGPT2	Angiopoietin 2	.42
59	205016_at	HU133p2_14464	NM_003236	TGFA	Transforming growth factor, alpha	.42
60	238469_at	HU133p2_47719	BE620374	OGFRL1	Opioid growth factor receptor-like 1	.42
61	209541_at	HU133p2_18955	AI972496	IGF1	Insulin-like growth factor 1 (somatomedin C)	.42
62	213004_at	HU133p2_22308	AI074333	ANGPTL2	Angiopoietin-like 2	.41
63	205463_s_at	HU133p2_14911	NM_002607	PDGFA	Platelet-derived growth factor alpha polypeptide	.41
64	222860_s_at	HU133p2_32140	AB033832	PDGFD	Platelet-derived growth factor D	.41
65	213001_at	HU133p2_22305	AF007150	ANGPTL2	Angiopoietin-like 2	.41
66	203426_s_at	HU133p2_12874	M65062	IGFBP5	Insulin-like growth factor–binding protein 5	.41
67	209652_s_at	HU133p2_19062	BC001422	PGF	Placental growth factor	.40
68	209410_s_at	HU133p2_18824	AF000017	GRB10	Growth factor receptor-bound protein 10	.39
69	206589_at	HU133p2_16036	NM_005263	GFI1	Growth factor independent 1 transcription repressor	.36
70	211577_s_at	HU133p2_20903	M37484	IGF1	Insulin-like growth factor 1 (somatomedin C)	.35
71	219514_at	HU133p2_28799	NM_012098	ANGPTL2	Angiopoietin-like 2	.35
72	204659_s_at	HU133p2_14107	AF124604	GFER	Growth factor, augmenter of liver regeneration	.35
73	201289_at	HU133p2_10738	NM_001554	CYR61	Cysteine-rich, angiogenic inducer, 61	.35
74	202841_x_at	HU133p2_12291	NM_007346	OGFR	Opioid growth factor receptor	.34
75	203627_at	HU133p2_13075	AI830698	IGF1R	Insulin-like growth factor 1 receptor	.33

(*Continued*)

Table 2. (*Continued*)

No.	Probe set ID	Probe ID	Representative public ID	Gene symbol	Gene title	Average log2 ratio
76	203002_at	HU133p2_12452	NM_016201	AMOTL2	Angiomotin-like 2	.33
77	222719_s_at	HU133p2_31999	AB033831	PDGFC	Platelet-derived growth factor C	.32
78	209747_at	HU133p2_19156	J03241	TGFB3	Transforming growth factor, beta 3	.31
79	210755_at	HU133p2_20137	U46010	HGF	Hepatocyte growth factor (hepapoietin A; scatter factor)	.30
80	205638_at	HU133p2_15086	NM_001704	BAI3	Brain-specific angiogenesis inhibitor 3	.30
81	209409_at	HU133p2_18823	D86962	GRB10	Growth factor receptor-bound protein 10	.29
82	206254_at	HU133p2_15701	NM_001963	EGF	Epidermal growth factor (beta-urogastrone)	.27
83	211535_s_at	HU133p2_20862	M60485	FGFR1	Fibroblast growth factor receptor 1	.27
84	211959_at	HU133p2_21267	AW007532	IGFBP5	Insulin-like growth factor–binding protein 5	.26
85	221976_s_at	HU133p2_31257	AW207448	HDGFRP3	Hepatoma-derived growth factor 2 (HDGF2)	.25
86	209651_at	HU133p2_19061	BC001830	TGFB1I1	Transforming growth factor beta 1–induced transcript 1	.25
87	208240_s_at	HU133p2_17665	NM_013394	FGF1	Fibroblast growth factor 1 (acidic)	.22
88	204682_at	HU133p2_14130	NM_000428	LTBP2	Latent transforming growth factor beta binding protein 2	.22
89	205572_at	HU133p2_15020	NM_001147	ANGPT2	Angiopoietin 2	.22
90	225330_at	HU133p2_34588	AL044092	IGF1R	Insulin-like growth factor 1 receptor	.21
91	228121_at	HU133p2_37376	AU145950	TGFB2	Transforming growth factor, beta 2	.21
92	209909_s_at	HU133p2_19316	M19154	TGFB2	Transforming growth factor, beta 2	.20
93	209101_at	HU133p2_18516	M92934	CTGF	Connective tissue growth factor	.19
94	215248_at	HU133p2_24543	AU145003	GRB10	Growth factor receptor-bound protein 10	.18
95	203084_at	HU133p2_12534	NM_000660	TGFB1	Transforming growth factor, beta 1	.18
96	224339_s_at	HU133p2_33607	AB056476	ANGPTL1	Angiopoietin-like 1	.16
97	209960_at	HU133p2_19367	X16323	HGF	Hepatocyte growth factor (hepapoietin A; scatter factor)	.16
98	1555103_s_at	HU133p2_02066	BC010956	FGF7	Fibroblast growth factor 7 (keratinocyte growth factor)	.16
99	208042_at	HU133p2_17472	NM_013303	AGGF1	Angiogenic factor with G patch and FHA domains 1	.15
100	230231_at	HU133p2_39486	BE549937	FGF14	Fibroblast growth factor 14	.14
101	228266_s_at	HU133p2_37521	BE703418	HDGFRP3	Hepatoma-derived growth factor, related protein 3	.14
102	210513_s_at	HU133p2_19904	AF091352	VEGFA	Vascular endothelial growth factor A	.13
103	223690_at	HU133p2_32967	AF113211	LTBP2	Latent transforming growth factor beta binding protein 2	.13
104	227308_x_at	HU133p2_36564	AW515704	LTBP3	Latent transforming growth factor beta binding protein 3	.12
105	220407_s_at	HU133p2_29692	NM_003238	TGFB2	Transforming growth factor, beta 2	.12
106	204422_s_at	HU133p2_13870	NM_002006	FGF2	Fibroblast growth factor 2 (basic)	.12
107	222112_at	HU133p2_31393	AV710549	EPS15L1	Epidermal growth factor receptor pathway substrate 15-like 1	.10
108	230681_at	HU133p2_39936	AI279879	TBRG1	Transforming growth factor beta regulator 1	.10
109	236034_at	HU133p2_45284	AA083514	ANGPT2	Angiopoietin 2	.10
110	209961_s_at	HU133p2_19368	M60718	HGF	Hepatocyte growth factor (hepapoietin A; scatter factor)	.10
111	203628_at	HU133p2_13076	H05812	IGF1R	Insulin-like growth factor 1 receptor	.10
112	205609_at	HU133p2_15057	NM_001146	ANGPT1	Angiopoietin 1	.07
113	215075_s_at	HU133p2_24370	L29511	GRB2	Growth factor receptor-bound protein 2	.07
114	205226_at	HU133p2_14674	NM_006207	PDGFRL	Platelet-derived growth factor receptor-like	.06

115	209526_s_at	HU133p2_18940	AB029156	HDGFRP3	Hepatoma-derived growth factor, related protein 3	.06
116	206987_x_at	HU133p2_16434	NM_003862	FGF18	Fibroblast growth factor18	.06
117	210999_s_at	HU133p2_20367	U66065	GRB10	Growth factor receptor-bound protein 10	.05
118	238453_at	HU133p2_47703	AI628573	FGFBP3	Fibroblast growth factor–binding protein 3	.04
119	201392_s_at	HU133p2_10841	BG031974	IGF2R	Insulin-like growth factor 2 receptor	.03
120	216867_s_at	HU133p2_26158	X03795	PDGFA	Platelet-derived growth factor alpha polypeptide	.02
121	215404_x_at	HU133p2_24699	AK024388	FGFR1	Fibroblast growth factor receptor 1	.02
122	225450_at	HU133p2_34708	AI433831	AMOTL1	Angiomotin-like 1	.01
123	202728_s_at	HU133p2_12177	AI986120	LTBP1	Latent transforming growth factor beta binding protein 1	.00
124	203821_at	HU133p2_13269	NM_001945	HBEGF	Heparin-binding EGF-like growth factor	.00
125	205110_s_at	HU133p2_14558	NM_004114	FGF13	Fibroblast growth factor 13	−.01
126	223049_at	HU133p2_32329	AF246238	GRB2	Growth factor receptor-bound protein 2	−.01
127	202409_at	HU133p2_11858	X07868	IGF2///INS-IGF2	Insulin-like growth factor 2 (somatomedin A)///INS-IGF2 readthrough transcript	−.03
128	231773_at	HU133p2_41028	BF002046	ANGPTL1	Angiopoietin-like 1	−.03
129	210428_s_at	HU133p2_19827	AF260566	HGS	Hepatocyte growth factor–regulated tyrosine kinase substrate	−.05
130	226705_at	HU133p2_35961	BE467261	FGFR1	Fibroblast growth factor receptor 1	−.05
131	203131_at	HU133p2_12580	NM_006206	PDGFRA	Platelet-derived growth factor receptor, alpha polypeptide	−.05
132	222164_at	HU133p2_31445	AU145411	FGFR1	Fibroblast growth factor receptor 1	−.07
133	219304_s_at	HU133p2_28589	NM_025208	PDGFD	Platelet-derived growth factor D	−.07
134	202729_s_at	HU133p2_12178	NM_000627	LTBP1	Latent transforming growth factor beta binding protein 1	−.07
135	216693_x_at	HU133p2_25984	AL133102	HDGFRP3	Hepatoma-derived growth factor, related protein 3	−.07
136	207937_x_at	HU133p2_17374	NM_023110	FGFR1	Fibroblast growth factor receptor 1	−.08
137	205302_at	HU133p2_14750	NM_000596	IGFBP1	Insulin-like growth factor–binding protein 1	−.09
138	38037_at	HU133p2_54303	M60278	HBEGF	Heparin-binding EGF-like growth factor	−.09
139	210512_s_at	HU133p2_19903	AF022375	VEGFA	Vascular endothelial growth factor A	−.09
140	225459_at	HU133p2_34717	AU157155	AMOTL1	Angiomotin-like 1	−.13
141	209524_at	HU133p2_18938	AK001280	HDGFRP3	Hepatoma-derived growth factor, related protein 3	−.13
142	218847_at	HU133p2_28132	NM_006548	IGF2BP2	Insulin-like growth factor 2 mRNA-binding protein 2	−.15
143	201494_at	HU133p2_10943	NM_005040	PRCP	Prolylcarboxypeptidase (angiotensinase C)	−.17
144	202609_at	HU133p2_12058	NM_004447	EPS8	Epidermal growth factor receptor pathway substrate 8	−.19
145	203820_s_at	HU133p2_13268	NM_006547	IGF2BP3	Insulin-like growth factor 2 mRNA-binding protein 3	−.22
146	212171_x_at	HU133p2_21478	H95344	VEGFA	Vascular endothelial growth factor A	−.23
147	201393_s_at	HU133p2_10842	NM_000876	IGF2R	Insulin-like growth factor 2 receptor	−.23
148	218718_at	HU133p2_28003	NM_016205	PDGFC	Platelet-derived growth factor C	−.25
149	211485_s_at	HU133p2_20813	AF211188	FGF18	Fibroblast growth factor 18	−.28
150	211568_at	HU133p2_20894	AB011122	BAI3	Brain-specific angiogenesis inhibitor 3	−.29
151	232680_at	HU133p2_41935	AI352424	HDGFL1	Hepatoma-derived growth factor-like 1	−.31
152	239183_at	HU133p2_48433	W67461	ANGPTL1	Angiopoietin-like 1	−.31
153	204379_s_at	HU133p2_13827	NM_000142	FGFR3	Fibroblast growth factor receptor 3	−.33
154	208441_at	HU133p2_17861	NM_015883	IGF1R	Insulin-like growth factor 1 receptor	−.33

(Continued)

Table 2. (*Continued*)

No.	Probe set ID	Probe ID	Representative public ID	Gene symbol	Gene title	Average log2 ratio
155	231031_at	HU133p2_40286	AI761573	KGFLP2	Keratinocyte growth factor–like protein 2	−.34
156	208228_s_at	HU133p2_17654	M87771	FGFR2	Fibroblast growth factor receptor 2	−.36
157	211029_x_at	HU133p2_20396	BC006245	FGF18	Fibroblast growth factor 18	−.38
158	209521_s_at	HU133p2_18935	AF286598	AMOT	Angiomotin	−.39
159	228699_at	HU133p2_37954	AI741712	NRP2	Vascular endothelial cell growth factor 165 receptor 2 (VEGF165R2)	−.40
160	211551_at	HU133p2_20877	K03193	EGFR	Epidermal growth factor receptor (erythroblastic leukemia viral (v-erb-b) oncogene homolog, avian)	−.42
161	204421_s_at	HU133p2_13869	M27968	FGF2	Fibroblast growth factor 2 (basic)	−.42
162	205782_at	HU133p2_15230	NM_002009	FGF7	Fibroblast growth factor 7 (keratinocyte growth factor)	−.44
163	205586_x_at	HU133p2_15034	NM_003378	VGF	VGF nerve growth factor inducible	−.44
164	203819_s_at	HU133p2_13267	AU160004	IGF2BP3	Insulin-like growth factor 2 mRNA-binding protein 3	−.47
165	215305_at	HU133p2_24600	H79306	PDGFRA	Platelet-derived growth factor receptor, alpha polypeptide	−.49
166	1554741_s_at	HU133p2_01794	AF523265	FGF7///KGFLP1///KGFLP2	Fibroblast growth factor 7 (keratinocyte growth factor)///keratinocyte growth factor–like protein 1	−.57
167	230288_at	HU133p2_39543	AW418619	FGF14	Fibroblast growth factor 14	−.64
168	209946_at	HU133p2_19353	U58111	VEGFC	Vascular endothelial growth factor C	−.82
169	230410_at	HU133p2_39665	N25995	NRP2	Vascular endothelial cell growth factor 165 receptor 2 (VEGF165R2)	−.91
170	206204_at	HU133p2_15651	NM_004490	GRB14	Growth factor receptor-bound protein 14	−.96
171	219803_at	HU133p2_29088	NM_014495	ANGPTL3	Angiopoietin-like 3	−1.10
172	231684_at	HU133p2_40939	AV659209	ANGPTL3	Angiopoietin-like 3, mRNA (cDNA clone IMAGE: 3934961)	−1.47
173	203638_s_at	HU133p2_13086	NM_022969	FGFR2†	Fibroblast growth factor receptor 2	−1.84
174	207750_at	HU133p2_17192	NM_018510	EPS15L2	Epidermal growth factor receptor pathway substrate 15-like 2	−2.22
175	206423_at	HU133p2_15870	NM_021146	ANGPTL7	Angiopoietin-like 7	−2.40

Abbreviations: cDNA, complementary DNA; mRNA, messenger RNA.
*More than 5 of comparison sets showing (log2 ratio ≥ 1 and the detection call of the highly calcified plaque "P").
†More than 5 of comparison sets showing (log2 ratio ≤ -1 and the detection call of the low-calcified plaque "P").

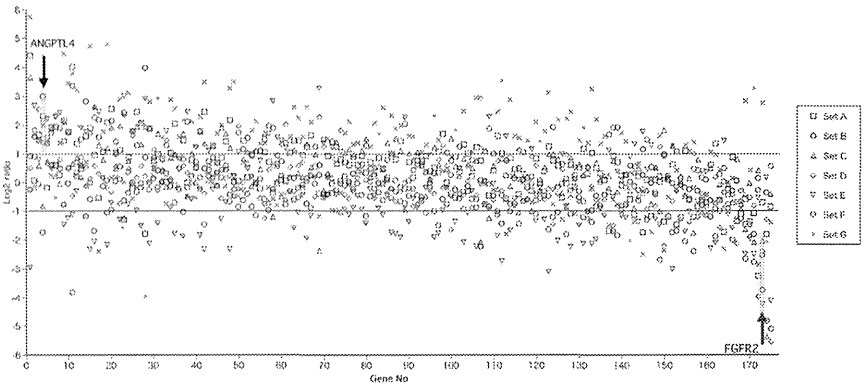

Figure 1. *Results of microarray analysis. GeneChip analysis showed 93 angiogenesis or growth factor–related transcripts reliably expressed (175 probe sets). Among them, ANGPTL4 and FGFR2 genes showed significant difference to fulfill the following criteria: (1) (log2 ratio ≥ 1 and the detection call of the highly calcified plaque "P [present]") in more than 5 of 7 comparison sets or (2) (log2 ratio ≤ −1 and the detection call of the low-calcified plaque "P") in more than 5 of 7 comparison sets. Gene numbers correspond to those shown in Table 2 in the order of average log2 ratio. Abbreviations: ANGPTL4, angiopoietin-like protein 4; FGFR2, fibroblast growth factor receptor 2.*

(Roche Diagnostics) mix solution and were run in duplicate in a LightCycler480 (Roche Diagnostics) (1 cycle at 95°C for 10 min, 40 cycles at 95°C for 10 s, 60°C for 10 s, and 72°C for 10 s (target genes) or 20 s (β-actin). The amplified transcripts were quantified by comparative computed tomography method using human β-actin as the internal control. The primer sequences on the basis of GenBank accession numbers were as follows: human angiopoietin-like protein 4 (ANGPTL4; NM_139314.1, 124 bp)—forward: 5′-ACT TGG GAC CAG GAT CAC GA-3′ and reverse: 5′-GTG GGA TGG AGV GGA AGT-3′; human fibroblast growth factor receptor 2 (FGFR2; NM_000141.4, 98 bp)—forward: 5′-AAC GGG AAG GAG TTT AAG CA-3′ and reverse 5′-TTG TCA GAT GGG ACC ACA CT-3′.

Western Blotting

Three high-calcified plaques (H7: 911.1, H8: 680.9, H9: 614.0) and 3 low-calcified plaques (L7: 26.6, L8: 55.5, L9: 83.5) were used for Western blotting analysis. Total cellular proteins were isolated with T-PER tissue protein extraction reagent (Thermo Scientific, Pierce Biotechnology, Rockford, IL). Proteins were quantitated by BCA protein assay reagent (Pierce Biotechnology), and equal amounts of protein from each sample (10 μg per lane) were separated on 10% sodium dodecyl sulfate–polyacrylamide gel electrophoresis followed by electroblotting to polyvinylidene difluoride membranes (Hybond P; GE Healthcare, Buckinghamshire, UK). Membranes were blocked in 1% skimmed milk and .1% Tween 20 in phosphate-buffered saline. ANGPTL4 was detected using mouse polyclonal antibody (1:500; Abnova, Taipei, Taiwan). FGFR2 was detected using mouse monoclonal antibodies (1:200; Abnova). The secondary antibody was horseradish peroxidase–conjugated rabbit anti-mouse immunoglobulin (IgG; 1:400,000; Millipore, Merck Millipore, Billerica, MA). Proteins were visualized using ECL Plus Western Blotting Detection Reagents (GE Healthcare). Semiquantitative analysis of protein concentration from Western blots was performed using a scanner with analyzing software (Scion Image; Scion Co., Frederick, MD).

Immunohistochemistry

The same plaques used in Western blotting analysis were also applied for immunohistochemistry. Paraformaldehyde-fixed sections of the specimens were embedded in paraffin. The sections were deparaffinized, rinsed in Tris-buffered saline (TBS), and treated with .3% hydrogen peroxide in methanol (30 min at room temperature). Slides were placed in DAKO Protein Block (Dako, Glostrup, Denmark) for 10 minutes before Avidin/Biotin Blocking Kit (SP-2001; Vector Laboratories, Burlingame, CA) was applied. Primary antibodies (ANGPTL4 mouse monoclonal antibody, 1:500, ALX-804-723; ENZO Life Sciences, Farmingdale, NY; FGFR2 mouse monoclonal antibody, 1:500, Abnova H00002263-M01) were added, and sections were incubated overnight at 4°C. Anti-rabbit Biotin (E0432; Dako) was applied following rinsing in TBS, and the slides were incubated for 30 minutes at room temperature. The streptavidin–peroxidase complex (426062; Nichirei, Tokyo, Japan) was then used, and the sections were incubated for 5 minutes followed by rinsing in TBS. Diaminobenzidine was used as the chromogen and counterstained with hematoxylin. Mouse IgG1 (X0931; Dako) and Mouse IgG2b (MAB0042; R&D Systems, Minneapolis, MN) served as negative controls, respectively.

Statistical Analysis

All statistical evaluations were performed with statistical software (Statview version 5.0; SPS, NC), and all results are presented as mean ± SEM values. The Mann–Whitney *U* test was used to compare the expression of real-time PCR and the signal intensities of Western blotting analysis for high- and low-calcified plaques and to compare the degrees of stenosis between them. Values of *P* less than .01 were considered significant.